LAWRENCE
LIVERMORE
NATIONAL
LABORATORY

LLNL-PROC-696137

Combined Neutron and X-ray Imaging at the National Ignition Facility

C. R. Danly, K. S. Christensen, V. E. Fatherley, D. N. Fittinghoff, G. P. Grim, R. L. Hibbard, N. Izumi, D. Jedlovec, F. E. Merrill, K. Skulina, P. L. Volegov, C. H. Wilde

June 29, 2016

High-Temperature Plasma Diagnostics 2016 Conference
Madison, WI, United States
June 5, 2016 through June 9, 2016

Disclaimer

This document was prepared as an account of work sponsored by an agency of the United States government. Neither the United States government nor Lawrence Livermore National Security, LLC, nor any of their employees makes any warranty, expressed or implied, or assumes any legal liability or responsibility for the accuracy, completeness, or usefulness of any information, apparatus, product, or process disclosed, or represents that its use would not infringe privately owned rights. Reference herein to any specific commercial product, process, or service by trade name, trademark, manufacturer, or otherwise does not necessarily constitute or imply its endorsement, recommendation, or favoring by the United States government or Lawrence Livermore National Security, LLC. The views and opinions of authors expressed herein do not necessarily state or reflect those of the United States government or Lawrence Livermore National Security, LLC, and shall not be used for advertising or product endorsement purposes.

Combined Neutron and X-ray Imaging at the National Ignition Facility

C. R. Danly,[1] K. Christensen,[2] V. E. Fatherley,[1] D. N. Fittinghoff,[2] G. P. Grim,[2] R. Hibbard,[2] N. Izumi,[2] D. Jedlovec,[2] F. E. Merrill,[1] D. W. Schmidt,[1] R. A. Simpson,[1] K. Skulina,[2] P. L. Volegov,[1] and C. H. Wilde[1]
[1)] *Los Alamos National Laboratory, Los Alamos, New Mexico 87544, USA*
[2)] *Lawrence Livermore National Laboratory, Livermore, California 94550, USA*

X-ray and neutrons are commonly used to image Inertial Confinement Fusion implosions, providing key diagnostic information on the fuel assembly of burning DT fuel. The x-ray and neutron data provided are complementary as the production of neutrons and x-rays occur from different physical processes, but typically these two images are collected from different views with no opportunity for co-registration of the two images. Neutrons are produced where the DT fusion fuel is burning; X-rays are produced in regions corresponding to high temperatures. Processes such as mix of ablator material into the hotspot can result in increased x-ray production and decreased neutron production but can only be confidently observed if the two images are collected along the same line of sight and co-registered. To allow direct comparison of x-ray and neutron data, a Combined Neutron X-ray Imaging system has been tested at Omega and installed at the National Ignition Facility to collect an x-ray image along the currently installed neutron imaging line-of-sight. This system is described, and initial results are presented along with prospects for definitive coregistration of the images.

I. BACKGROUND AND MOTIVATION

Experiments conducted at the National Ignition Facility (NIF) aim to achieve nuclear fusion burn in inertially-confined plasmas generated by laser-driven implosion of fuel-filled capsules. In the typical configuration, a high-density cryogenic deuterium-tritium (DT) ice layer is formed on the inside of a spherical plastic shell 1-2mm in diameter; the center of the capsule contains DT gas at the vapor pressure. When the capsule is imploded at velocities reaching 300km/s, this ice layer is compressed to extremely high density, and shock and compression heat the DT gas in the center to multi-keV temperatures, causing fusion reactions. If the density of the surrounding cold fuel is sufficiently high, alpha particles emanating from the hotspot should deposit their energy in a small region of this fuel, heating it to thermonuclear temperatures and producing a propagating fusion burn. However, experimental yields fall far short of simulation. Hydrodynamic mix at the shell-fuel and fuel-gas interfaces, ion kinetic effects, or other processes may contribute to the failure of these capsules to achieve ignition. Therefore, improving the understanding of this fuel assembly near the time of peak compression or stagnation is crucial.

A. X-ray imaging

X-ray imaging is a well-established diagnostic technique in inertial confinement fusion (ICF) and an area of continuing development[1,2]. Typically, x-ray emission from the source is imaged through an array of pinholes in a tantalum foil, onto a microchannel-plate detector with a segmented gate electrode; each pinhole image is recorded at a different time, providing a time history of the source emission. Other techniques such as Kirkpatrick-Baez optics can also be used, and faster time-resolved detectors are being developed[3].

B. Neutron Imaging

The Neutron Imaging System (NIS) at NIF records neutrons produced by the fusion reactions taking place in the target[4,5]. A tungsten-and-gold aperture array placed 32.5cm from the target forms pinhole and coded-aperture penumbral neutron images on a pixellated fiber scintillator array 28m away in the neutron imaging annex. The visible light images produced in this scintillator are recorded by a pair of fast-gated intensified camera systems. The long line of sight provides enough magnification to overcome limits in scintillator resolution, and also allows imaging in multiple energy bins. The neutrons are all produced in a relatively short burn time on the order of 100ps, while the transit times to the detector for 10 and 14 MeV neutrons vary by 100ns. Typically, the lens-coupled camera records primary neutrons in the 13-17 MeV energy range, and the fiber-coupled camera is timed to capture neutrons which have downscattered from their birth energy to 6-12 MeV; both cameras record the entire scintillator. This system is described in detail in Merrill *et al.*[5]. The primary image identifies the location of fusion reactions in the capsule, and the downscattered image provides information about the location of high-density material near this hotspot[6].

In contrast to x-rays, 14 MeV neutrons are highly penetrating even through high-Z materials. As a result the traditional planar pinhole must be replaced by a thick high-Z aperture. The NIF neutron imaging aperture consists of pinholes and penumbral apertures cut into the length of a 20cm thick gold slab. The pinholes are equilateral triangular grooves which open from a point at the target-facing end of the aperture to 210μm depth at the detector-facing end; the penumbral apertures are double-tapered truncated cones with a diameter of 273μm at the target-facing end, 300μm at the halfway point, and 437μm at the detector-facing end. Manufacturing technology limitations and the 3D nature of the aperture array mean that shift-variant distortions are introduced

into the images. These distortions must be corrected to produce usable images of the source; this is accomplished by reconstruction using iterative maximal likelihood algorithms described in Volegov *et al.*[7].

C. Motivation for comparing x-rays and neutrons

Neutrons and high energy (Bremsstrahlung) x-rays are both emitted from the hot DT plasma, and for symmetric implosions with no carbon mix, the neutron and x-ray images reflect similar regions. This can be seen in the 2011 data shown in Figure 1. Neutron and x-ray emission carry different dependence on the plasma conditions. The neutron emission depends on DT ion density and is extremely sensitive to ion temperature. X-ray emission also depends on ion density and electron density, but varies with electron temperature and increases as Z^2. Carbon mixed into the fuel from the ablator increases bremsstrahlung x-ray emission, but lessens the temperature resulting in reduced neutron emission. Additionally, only a small fraction of the neutrons emitted by the hotspot are scattered by the surrounding fuel mass, but attenuation for x-rays can be significant, up to $\sim 50\%$. Differences between neutron and x-ray images are diagnostic signatures of mix and areal density asymmetries.

Qualitative asymmetries and differences between neutron and x-ray images have been observed in some experiments. Synthetic images from a post-shot simulation of one such shot, N140311, are shown in Figure 2; a high-mix region in the simulation is visible in these as increased x-ray and reduced neutron emission in the upper right side of the source. Such comparison in data could provide valuable information on mix and asymmetry in NIF implosions. However, existing neutron and x-ray imagers view the target from different lines of sight. The NIS is located on the equator at 315 degrees azimuthal angle, while the primary x-ray imagers are located 123 degrees away on the equator at 78 degrees, and 90 degrees away at the north pole. As a result, for asymmetric implosions, comparison of features between these images can be ambiguous or impossible. Therefore, a technique was developed to record neutron and x-ray images simultaneously along the same, existing neutron imaging line of sight, to facilitate direct comparison.

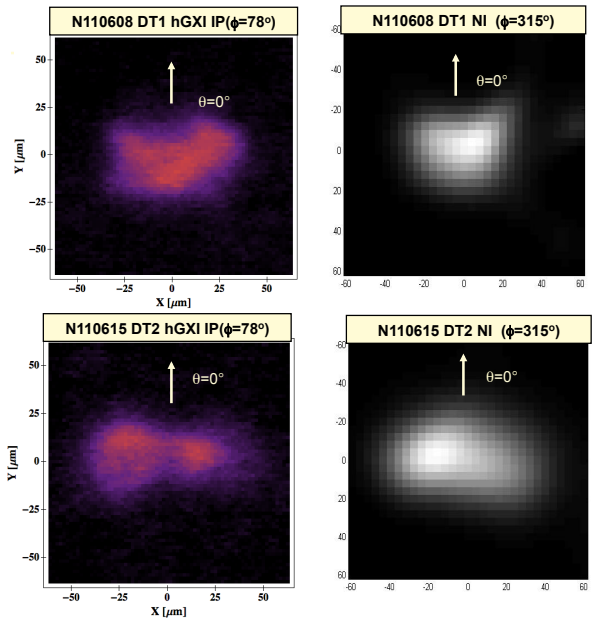

FIG. 1. Neutron and x-ray images are similar for simple, clean implosions, such as NIF shots N110608 and N110615.

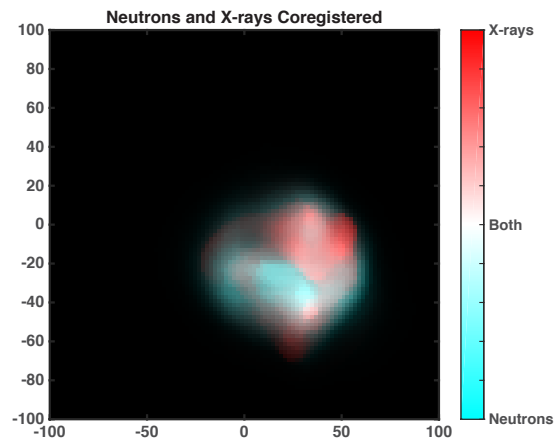

FIG. 2. Synthetic neutron and x-ray images along the same line of sight, from 3D simulations of a highly-asymmetric NIF shot by Spears *et al.*[8]

II. COMBINED NEUTRON AND X-RAY IMAGING

In theory, it should be possible to construct an aperture array which forms both neutron and x-ray images using the same physical edge[9]. However, the pinholes in the current NIF neutron imaging array taper to zero depth and are closed at the end facing the target. This results in improved resolution for the neutron imaging, but makes the pinholes completely opaque to x-rays. Further, because of the vast difference in scattering/attenuation length (4.5μm for 10 keV photons versus 3.2cm for 14 MeV neutrons in gold[10]), x-rays experience a significantly different transmission profile than the neutrons passing through the same object. Micron-scale defects in the imaging edge of a penumbral aperture do not alter the aperture's performance for neutrons, but technological limitations make it impossible to characterize these edges precisely enough to correct for the distortions introduced in x-ray images. Such effects can be seen in Figure 3, and would likely be present in an open-ended neutron pinhole as well. The precision EDM and laser drilling techniques

used to produce x-ray pinholes are not suitable for thick apertures required for neutrons.

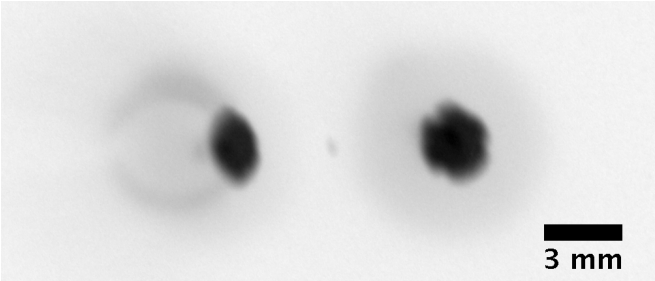

FIG. 3. Raw CNXI image plate x-ray data from Omega shot 74577. Source is outside field of view of left aperture. CNXI pinhole image is visible at center, and distortions due to penumbral aperture edge deviation from circular are visible in the right image.

One solution is to cover the existing neutron penumbral apertures with x-ray pinholes produced with the standard techniques, with the neutron apertures, for purposes of x-ray imaging, serving as extremely thick collimators[11]. The thin high-Z foil used for the x-ray pinholes does not affect the neutron imaging performance of the system, and the thick neutron imaging aperture does not obstruct the x-ray images as long as the source is in the clear-aperture field of view of the penumbra. A passive detector installed along the line of sight, inside the vacuum chamber, records x-ray images but again has minimal effect on the transmission of neutrons through to the neutron imaging system downstream. This combined neutron and x-ray imaging (CNXI) technique is illustrated in Figure 4.

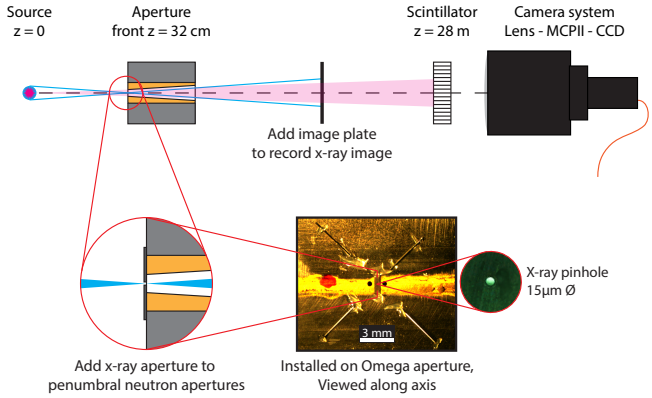

FIG. 4. Overview of CNXI concept (not to scale). A thin tantalum foil with x-ray pinhole is added covering the penumbral aperture of the neutron imaging system. The x-rays are recorded on image plates within the vacuum chamber, and the neutrons propagate unimpeded through to the existing NIS detector. Inset photo: X-ray pinhole installed on Omega aperture, viewed from downstream end.

III. TESTING AT OMEGA

This new technique was demonstrated at Omega in 2014. A duplicate of the penumbral layers of the NIF aperture array was constructed, and a tantalum foil with a 15μm pinhole was placed over the back of the central penumbra completely covering it. An image plate detector located in the target chamber, 3.5m from the chamber center (TCC), recorded x-ray images, and the Omega NIS located 10m further downstream on the same line of sight recorded neutron images. Existing x-ray framing cameras were fielded on one opposing and one orthogonal port to validate the performance of the CNXI system on a series of asymmetrically driven implosions. Data from this test is shown in Figure 5. As expected for this type of implosion, the x-ray images were slightly larger than the neutron images and tracked in shape as the drive asymmetry was varied; the results are detailed in Danly *et al.*[12]

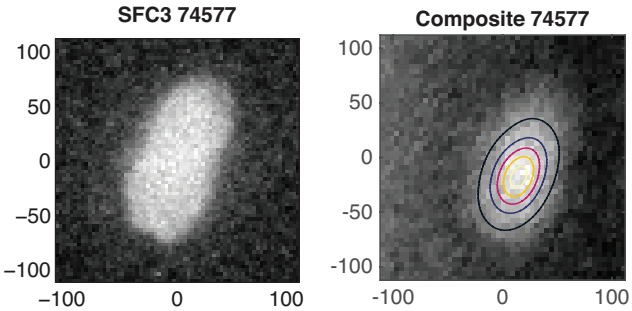

FIG. 5. Data from prolate-driven Omega shot 74577. Left: Time-resolved SFC3 image from opposing port, flipped for comparison. Right: CNXI time-integrated x-ray image with NIS reconstructed neutron source contours overlaid based on peak location. The CNXI image appears smaller and more centrally peaked due to the time-integration of an imploding hotspot. Spatial scales in μm.[12]

It was originally intended for the two uncovered neutron penumbras to provide position information for the x-ray source. It was determined, however, that as discussed in Section II, the image-forming central edge of the penumbral neutron apertures was neither sufficiently circular nor sufficiently well-characterized to allow its use in x-ray imaging. Therefore two additional x-ray pinholes were added to the design, covering the other penumbral apertures.

Statistical simulations showed that the optimal balance of signal-to-noise ratio and resolution for NIF yields, within the constraints of the NIS line of sight, is obtained with a pinhole diameter of 15μm.

IV. IMPLEMENTATION AT NIF

A. Aperture

After further testing at Omega, a set of x-ray pinholes were fabricated and installed on the NIF neutron imaging aperture. One pinhole was placed on the back of the aperture, covering the central penumbra, and pair of pinholes were placed on the front of the aperture covering the two outer penumbra. These added pinholes provide images with a higher magnification and information on source position, as discussed in Section VI A. The NIF neutron imaging aperture is shown before and after installation in Figure 6.

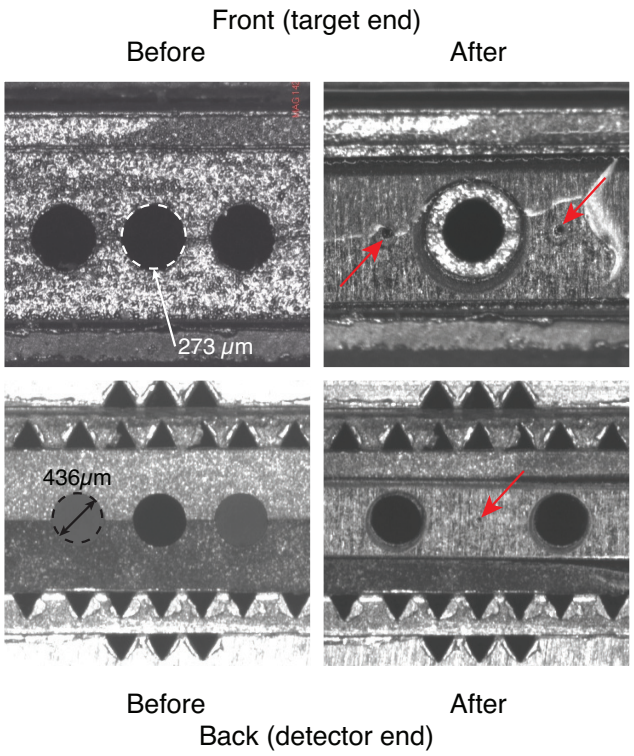

FIG. 6. X-ray pinholes installed on NIF aperture. Top row: Front (target-facing) end of aperture, before and after installation, with pinholes covering outer penumbra. Bottom row: back (detector-facing) end of aperture, before and after installation of x-ray pinhole covering center penumbra. X-ray pinholes indicated by red arrows. Spatial scales differ between top and bottom rows.

B. Detector stack

As in the Omega system, image plates are used to record time-integrated x-ray images inside the target chamber vacuum. In the NIF application, a detector pack is mounted inside the vacuum door at the back of DIM 90-315, on the NIS line of sight, 11.6 meters from the target. This location provides easy access to change the detector pack, and sufficient magnification to record high-quality x-ray images even with the relatively large target-to-pinhole distance in CNXI as compared to typical dedicated x-ray imagers.

A black Kapton film is used to block visible light from the image plates; The first image plate in this aluminum housing records x-ray images on a low neutron background; subsequent image plates paired with polyethylene converters record usable energy-integrated neutron images, as shown in Figure 9. This type of detector stack is being further developed for use in an energy-integrated short line of sight NIS for implementation on other lines of sight at NIF[13].

FIG. 7. NIF CNXI detector stack. Black kapton light-block followed by 6 layers of image plates interleaved with polyethylene converters for neutrons. Aluminum filter shown below black kapton was used only for N150820.

C. Line-of-sight modifications

In order to permit x-ray transmission from the target to the CNXI detector pack, modifications were required to the line of sight. The existing NIS blast shield, which protects the pinhole array from debris wind and ablation during the shot, was steel and opaque to the x-rays of interest. After examining other options such as beryllium and aluminum, a 1 mm-thick, single-use polycarbonate shield was selected. This provides $> 50\%$ transmission at energies over 10 keV. Additionally, a diagnostic window is required in the hohlraum for CNXI shots. This window was qualified and has been used on two diagnostic development shots, without measurable adverse effects on implosion symmetry or yield.

D. System performance

The front pinholes are located at 32.5 cm from TCC, and the back pinholes are 52.5cm from TCC, producing images at the detector with magnifications of $\sim 35\times$ and $\sim 21\times$, respectively. The image plate is scanned with a pixel size of 50μm, equivalent to its physical resolution. This gives a detector pixel size in the source plane of 1.4 and 2.4μm for the front and back pinholes, respectively. The pinhole size of 15μm was selected as the optimal tradeoff between resolution and signal level for the current NIF aperture and yields. This results in an SNR of 22 in the brightest portion of the image and ~ 5 at the 17% intensity contour; the low-intensity SNR is limited by detector neutron background. Post-processed x-ray image spatial resolution is estimated at better than 10 μm. The polycarbonate blast shield provides sufficient filtration for typical shots, but additional filtration can be added in the detector pack if needed. The spectral sensitivity of the system is shown in Figure 8.

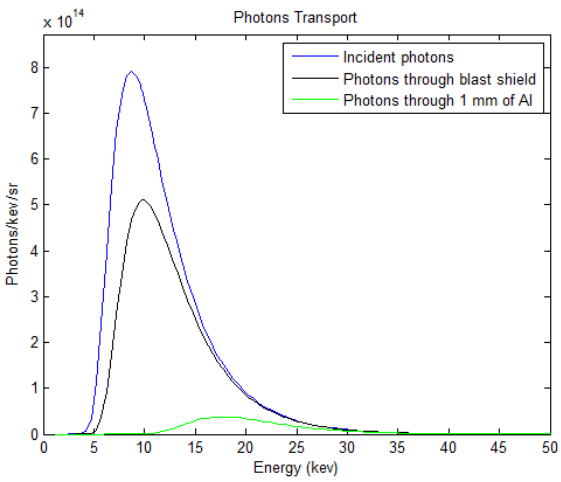

FIG. 8. NIF source spectrum and transmission of line of sight. Additional filtration can be added if needed.

V. DATA AND ANALYSIS

The CNXI system was commissioned on two diagnostic development shots, N150820 and N160210. These were DT gas-filled exploding pushers with no cryogenic ice layer, expected to produce images of the same size and shape for both primary neutrons and x-rays. Raw image plate data from N160210 is shown in Figure 9.The x-ray pinhole images fall in the central flat region of the neutron penumbral images and can be easily extracted. Because the x-ray image is only recorded by the first image plate, the subsequent image plates can be used to estimate and remove neutron background. Neutron data from the subsequent image plates (with polyethylene converters) are aligned and summed, and can be reconstructed as with the NIS camera system images. Legendre polynomials are then fit to the 17% intensity contour of the neutron and x-ray images for comparison.

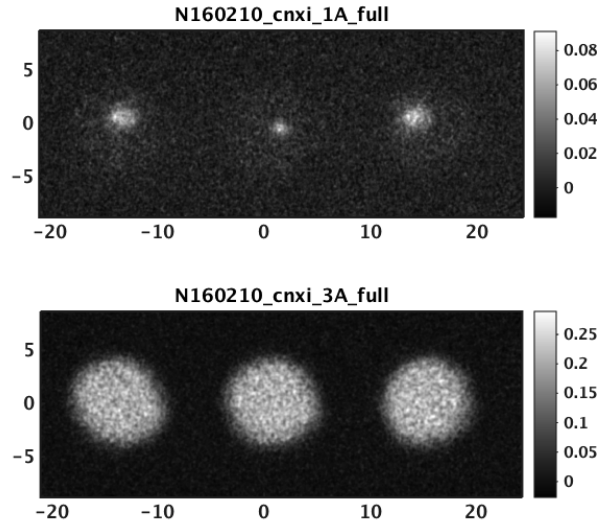

FIG. 9. Raw CNXI image plate data from N160210. Plate 1 records x-ray pinhole images on a low neutron background. Plate 2 records neutron penumbral images using polyethylene converter. Plates 3-6 record similar signal to second plate and can be summed to improve statistics. Note difference in neutron signal intensity between first image plate (no polyethylene) and second image plate (with polyethylene).

VI. COREGISTRATION

For simple sources such as the ones shown in Figures 5, it may be sufficient to simply overlay the neutron and x-ray images based on the location of peak intensity, or the image centroid. In the case of an asymmetric fuel or mix distribution, however, this could be misleading. In the simulated images of Figure 2, the neutron and x-ray emission peaks are roughly 20 μmapart; aligning the images in this way would obscure the physics of the fuel assembly. It is therefore necessary to definitively align or coregister the images.

It is theoretically possible to directly register the detectors and sources. However, few-micron surveying accuracy over a 28-meter line of sight would be required, and is currently not technically feasible.

Coregistration is instead achieved by independently determining the position of the x-ray source and the neutron source, relative to a common axis, from the respective data alone. The source location (i.e. implosion center) varies varies from shot to shot relative to the NIS/CNXI aperture, so the positions must be determined from a single set of images.

A. Determination of neutron source location

The neutron source position can be determined using a simplified version of the reconstruction algorithm discussed above; rather than fitting to an arbitrary source distribution, a uniform spheroid is projected through the aperture transmission matrix and position and size are varied to best fit the data. Errors in the knowledge of the aperture array geometry can induce systematic errors in this position; these are estimated at 2 μm. Statistical variation in the fit introduces random error as well, estimated at 5 μm.

B. Determination of x-ray source location

X-ray source position is determined by using pinholes with two different magnifications. As illustrated in Figure 11, this results in changes in the image spacing directly proportional to the source position relative to the axis[9]. With precise knowledge of the pinhole positions on the aperture array, the source position can be determined relative to the penumbral axis.

Stated differently, the three pinholes project the same image onto the detector, with a difference in scale and translation. By determining the transformation required to align these three identical images, the transformation from image plane to source plane coordinate systems is also uniquely determined, to within the noise.

Errors in aperture geometry knowledge again introduce systematic errors. For a reasonable pinhole placement error of 3 μm, this systematic error is estimated at 8 μm. Statistical error due to the determination of the image location is estimated at 5 μm.

C. Accuracy

The neutron penumbral apertures form images on the central edge, in the middle of the aperture, while the position of the x-ray pinholes is measured relative to the ends of the penumbral apertures. Deviations from straight in these apertures can induce a small additional error in the coregistration accuracy, which is estimated to be 4μm.

Metrology data from the installation of the x-ray pinholes on the apertures is currently insufficient for the coregistration purposes described above. However, a technique was developed to characterize the neutron aperture geometry, which is considerably more complex, using a global optimization over many shots[14]. This technique can be applied to the present problem, and should meet the accuracy requirements soon. With this data, overall coregistration accuracy should be better than 12μm RMS, or approximately one resolution element.

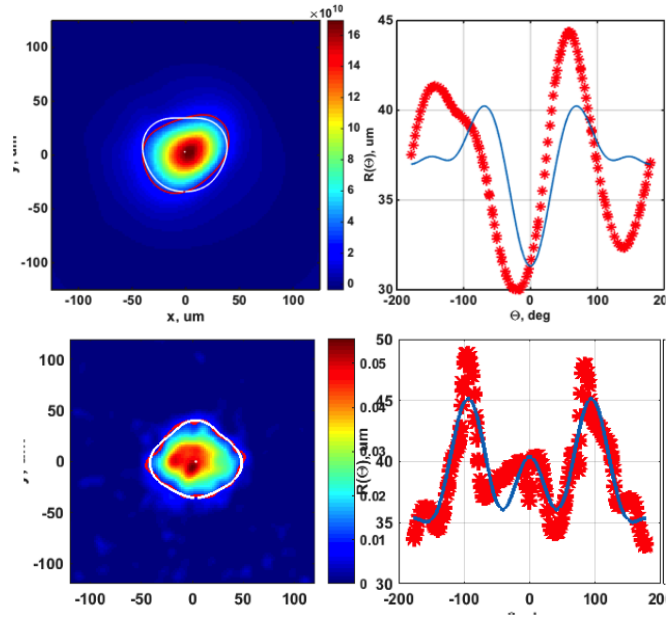

FIG. 10. NIS Neutron (top) and CNXI x-ray (bottom) images with contour fits for N160210. Source shape and size agree to within error bars as expected for this type of shot.

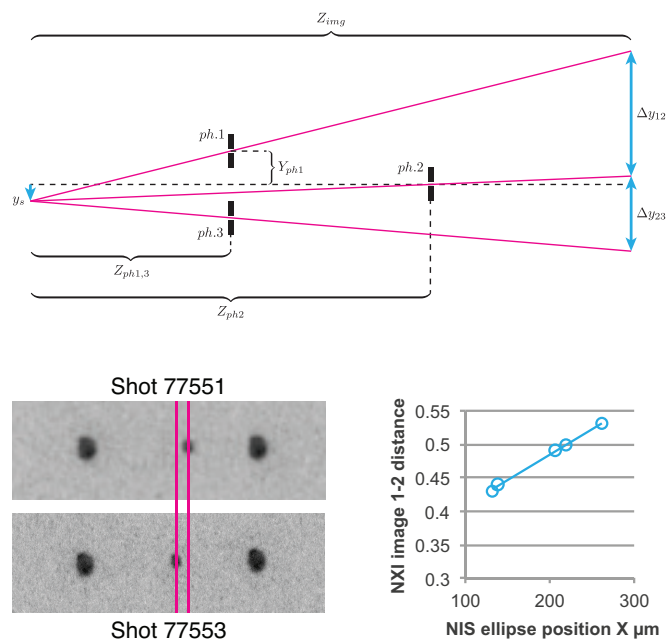

FIG. 11. Top: Determination of x-ray pointing using dual-magnification technique. With precise knowledge of pinhole positions, measured spacing of images $\Delta y'_{12}$ and $\Delta y'_{23}$ give source position y_s relative to axis of aperture array. Relative position of source plane coordinate system y and image plane coordinate system y' is not known a priori. Bottom left: example images from 3-pinhole array for two different Omega shots, showing variation in image spacing. Bottom right: x-ray image spacing tracks with neutron pointing solution as aperture array is moved relative to TCC for 5 shots.

VII. CONCLUSION

An x-ray imaging capability has been added to the existing neutron imaging system line of sight at NIF. This combined system provides simultaneous neutron and x-ray imaging along a single line of sight, with a spatial resolution of $\sim 10\mu$m. Further characterization of the aperture array will allow definitive coregistration of these neutron and x-ray images to within one resolution element. Separate algorithms recently developed enable the quantitative reconstruction of fuel mass density from combined analysis of primary and downscattered neutron images[15]. This will enable the CNXI x-ray images to be corrected for absorption in the fuel assembly, providing a more accurate picture of emission. Together, primary neutrons, reconstructed cold fuel density, and x-ray emission, will provide a detailed understanding of stagnation-time physics along the NIS line of sight.

Prepared by LLNL under Contract DE-AC52-07NA27344.

[1] D. K. Bradley, P. M. Bell, O. L. Landen, J. D. Kilkenny, and J. Oertel, Review of Scientific Instruments **66**, 716 (1995).
[2] J. A. Oertel *et al.*, Review of Scientific Instruments **77**, 10E308 (2006).
[3] S. R. Nagel *et al.*, Review of Scientific Instruments **83**, 10E116 (2012).
[4] M. D. Wilke *et al.*, Review of Scientific Instruments **79**, 10E529 (2008).
[5] F. E. Merrill *et al.*, Review of Scientific Instruments **83**, 10D317 (2012).
[6] G. P. Grim, N. Guler, F. E. Merrill, G. L. Morgan, C. R. Danly, P. L. Volegov, C. H. Wilde, D. C. Wilson, *et al.*, Physics of Plasmas (1994-present) **20**, 056320 (2013).
[7] P. Volegov, C. R. Danly, D. N. Fittinghoff, G. P. Grim, N. Guler, N. Izumi, T. Ma, F. E. Merrill, A. L. Warrick, C. H. Wilde, and D. C. Wilson, Review of Scientific Instruments **85**, 023508 (2014).
[8] B. K. Spears, D. H. Munro, S. Sepke, J. Caggiano, D. Clark, R. Hatarik, A. Kritcher, D. Sayre, C. Yeamans, J. Knauer, T. Hilsabeck, and J. Kilkenny, Physics of Plasmas **22**, 056317 (2015), http://dx.doi.org/10.1063/1.4920957.
[9] C. R. Danly, G. P. Grim, N. Guler, M. H. Intrator, F. E. Merrill, P. Volegov, and C. H. Wilde, Review of Scientific Instruments **83**, 10E522 (2012).
[10] Because of the large collimation of the neutron imaging line of sight (and aperture itself), the probability of a neutron scattered in the aperture arriving at the detector is negligible. Therefore, scattering in the aperture can be treated as absorption.
[11] F. E. Merrill, C. R. Danly, N. Izumi, D. Jedlovec, D. N. Fittinghoff, G. P. Grim, A. Pak, H.-S. Park, P. L. Volegov, and C. H. Wilde, Review of Scientific Instruments **85**, 11E614 (2014).
[12] C. R. Danly, T. H. Day, D. N. Fittinghoff, H. Herrmann, N. Izumi, Y. H. Kim, J. I. Martinez, F. E. Merrill, D. W. Schmidt, R. A. Simpson, P. L. Volegov, and C. H. Wilde, Review of Scientific Instruments **86**, 043503 (2015), http://dx.doi.org/10.1063/1.4918285.
[13] R. Simpson, K. Christensen, C. Danly, V. E. Fatherley, D. Fittinghoff, G. P. Grim, N. Izumi, D. Jedlovec, F. E. Merrill, K. Skulina, P. Volegov, and C. Wilde, Review of Scientific Instruments **86**, 125112 (2015), http://dx.doi.org/10.1063/1.4938543.
[14] P. L. Volegov, C. R. Danly, D. N. Fittinghoff, N. Guler, F. E. Merrill, and C. H. Wilde, Review of Scientific Instruments **85**, 123506 (2014).
[15] P. L. Volegov, D. T. Casey, C. R. Danly, F. E. Merrill, and C. H. Wilde, "Extracting cold-fuel volume density information from primary and down scattered neutron images," Forthcoming.